Supporting Information

Voltage Scaling of Graphene Device on $SrTiO_3$ Epitaxial Thin Film

Jeongmin Park,[†,‡,⊥] *Haeyong Kang,*[‡,⊥] *Kyeong Tae Kang,*[†,§,⊥] *Yoojoo Yun,*[†,‡] *Young Hee Lee,*[†,‡,§] *Woo Seok Choi,*[§,*] *Dongseok Suh*[†,‡,*]

[†] IBS Center for Integrated Nanostructure Physics, Institute for Basic Science, [‡] Department of Energy Science, [§] Department of Physics, Sungkyunkwan University, Suwon 440-746, Korea

[⊥] These authors contribute equally to this work.

[*] Corresponding authors: choiws@skku.edu; energy.suh@skku.edu

Estimation of contact resistance from two-terminal quantum Hall conductance

For a deeper understanding of the effect of atomically flat, high-*k* epitaxial thin film on the transport of graphene, we studied the quantum Hall conductance in this device. Even though the shape of the sample is not a Hall bar structure, the two-terminal quantum Hall conductance can be investigated at low temperatures under high magnetic fields. When the configuration of the two-terminal device is taken into account, several resistance components other than channel resistance (R_{CH}), such as wire resistance or contact resistance, could be added along the current pathway to give the measured resistance (R_{M}). Here, the sum of all subsidiary resistance components is regarded conceptually as a contact resistance ($\mathrm{R_C}$), and it gives the following relation;

$$R_{\mathrm{M}} = R_{\mathrm{CH}} + R_{\mathrm{C}} \ .$$

The measured data of conductance quantization under magnetic fields in our device is presented in Figure S1. We find that the resistance values of the quantized plateaus are different from the values corresponding to universal quantum Hall conductance that are expected in monolayer graphene. The difference is approximately 900 ohms for all quantized states, as indicated in Figure S1. If we assume that this difference originates from R_{C}, as suggested in the equation above, we can extract R_{CH} by simply subtracting the R_{C} value from R_{M}. Then the channel conductance becomes

$$G_{\mathrm{CH}}(T,H) = \frac{1}{R_{\mathrm{CH}}(T,H)} = \frac{1}{R_{\mathrm{M}}(T,H) - R_{\mathrm{C}}}$$

The R_C value does not vary much from 2 K to 200 K.

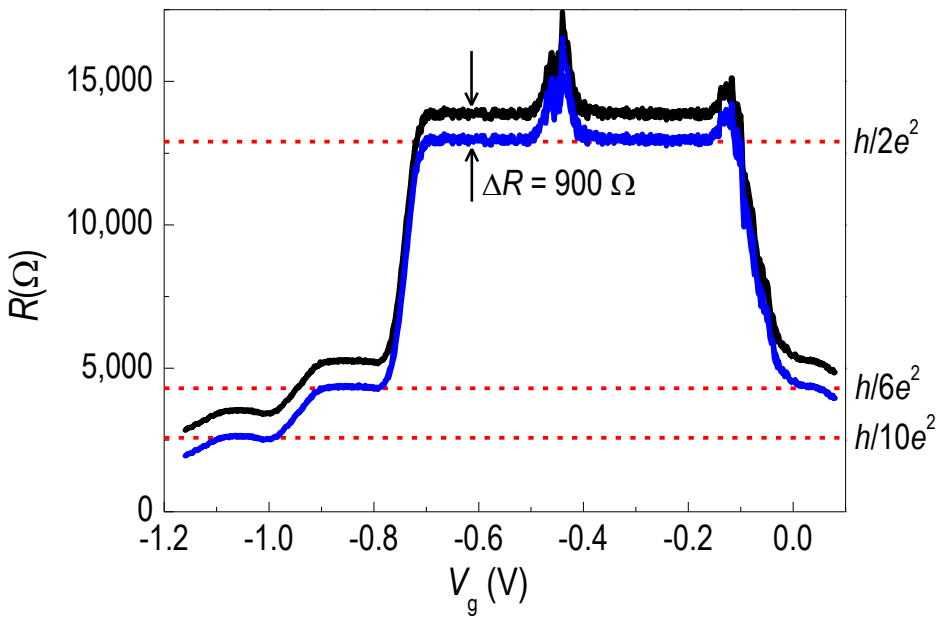

Figure S1. Comparison of experimental data in two-terminal resistance measurements under a magnetic field of 14 T with the theoretically expected quantized resistance values corresponding to quantum Hall states. The black curve indicates the measured data, and the blue curve is obtained after subtraction of 900 ohms from the measured data.

<u>Estimation of the effective dielectric constant of STO from two-terminal quantum Hall conductance and its temperature dependence</u>

The lower inset graph in Figure 5 indicates the method of using the quantum Hall plateaus to estimate the effective dielectric constant of the $SrTiO_3$ (STO) thin film. If we consider only the $\nu = 6$ state, the filling factor of this state should be matched with the quantized resistance plateau of

$G_{CH} = 6\ (e^2/h)$, which results in the range of ε_{eff} being approximately from 250 to 330 as presented in the lower inset of Figure 5.

For the temperature dependence of ε_{eff}, the location of the quantum Hall state transition from $\nu = 2$ to $\nu = 6$ was defined as ΔV_2 relative to the charge neutrality point (CNP) of V_{CNP}. For quantitative comparison, ΔV_2 is obtained from the first derivative of the conductance with respect to gate voltage under magnetic field between quantized resistance plateaus as illustrated in the upper inset of Figure 5. Because the carrier number to occupy the $\nu = 2$ state at fixed magnetic field is independent of temperature, little variation of ΔV_2 indicates that the effective dielectric constant also does not change much with temperature.

Leakage current pathway of the graphene device on STO thin film

For the leakage current path, there are three possibilities owing to the electrical contact made on the thin-film STO as seen in the inset of Figure 1c. The first is the Nb:STO/thin-film-STO/graphene, the second is the Nb:STO/thin-film-STO/Cr/Au, and the third is Nb:STO/thin-film-STO/silver-paste. In our work, it is not clear which one contributes most dominantly to the leakage current. In any case, Schottky contact behavior is clearly observed in the data presented in Figure 4a, which can be analyzed in terms of the schematic band diagrams shown in Figures S2a and S2b. The current flows relatively easily from Nb:STO to the top contact in the positive bias case (Figure S2a). On the other hand, for the negative bias, the current flow experiences a tunneling barrier due to a Schottky contact formed at the interface of the top contact and STO. For better

performance with respect to leakage current, adoption of suitable conducting substrates for epitaxial STO in addition to a well-defined top contact area should be examined as options to achieve ultra-high doping in atomically thin two-dimensional materials.

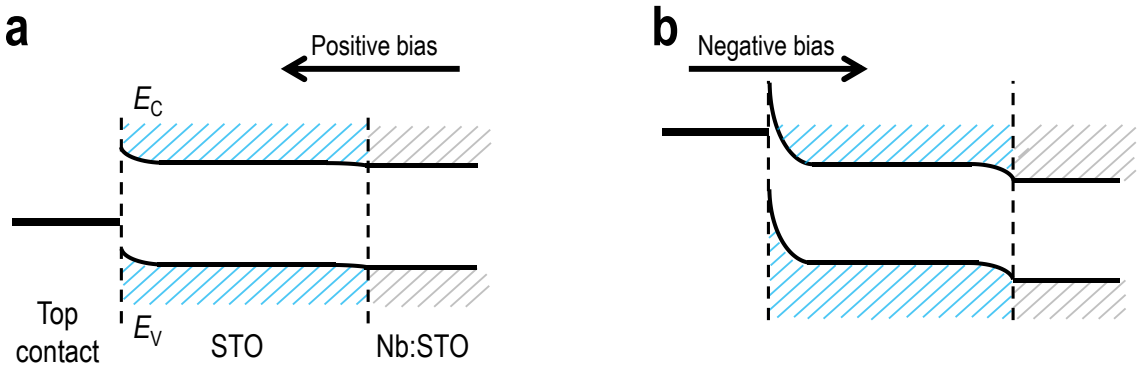

Figure S2. Schematic energy band diagram of the graphene-thin-film-STO device for (a) positive and (b) negative bias.

Carrier density dependent conductance of graphene

The conductance at 2 K shows a linear dependence in the vicinity of CNP but deviates from it as gate voltage increases as shown in Figure S3. Although there are still many debates on scattering mechanism affecting graphene transport, linear dependence on carrier density near CNP is considered to come from long-range Coulomb scattering.[25,30-33] The linear blue dotted lines in Figure S3 show that the conductance at low density is dominated by charged impurity scattering processes. As gate voltage increases, however, our data become fitted well with resonant scattering

mechanism by strong and short impurity potential as indicated by red lines in Figure S3.[1-5] The conductivity in the resonant scattering dominant region follows

$$\sigma = \frac{2e^2}{\pi h}\frac{\alpha V_g}{n_i}\ln^2\left(\sqrt{\pi\alpha V_g}r\right) \ ,$$

where α is the ratio of carrier density induced by gate voltage ($n = \alpha V_g$), n_i and r are the concentration and the potential range of resonant defects, respectively. We can roughly estimate the density of resonant scatterers from the fitting parameters as $2 \times 10^{12} cm^{-2}$ where r is set as 0.25 nm.

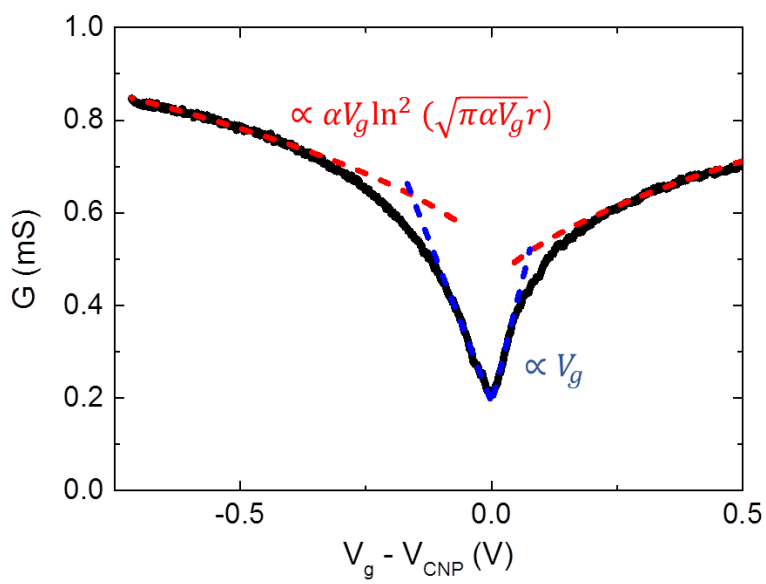

Figure S3. Gate voltage dependent conductance at 2 K. The blue and red dashed lines show linear and sublinear dependence on gate voltage, respectively.

Comparison of this work with others

The device structure and performance of this work and those of others in literature are summarized in Table S1.

	STO information						Graphene transport			
Ref.	Growth method	t (a)	Growth condition			Post-annealing	Hysteresis (ΔV_{CNP}) (b)	Quantum Hall states	$\lvert V(2I_{\mathrm{CNP}}) - V(I_{\mathrm{CNP}})\rvert$ (c)	ΔV_2 (d)
			$P(O_2)$	T	Laser fluence					
(Unit)	-	μm	mTorr	°C	J/cm^2	-	V	-	V	V
This work	PLD	0.3	100	700	1.3	400 Torr 400 °C, 1h	No hysteresis	Well-developed	0.06 (2 K) 0.4 (200 K)	0.3 (2 K)
[5]	bulk	500	-	-	-	-	No hysteresis	Well-developed	0.6 (0.25 K) 3.7 (50 K)	1.5 (0.25 K)
[6]	PLD	0.3	100	700	N/A	500 Torr 400 °C, 1h	1.5 (300K)	N/A	0.8 (300 K)	N/A
[7]	PLD	0.25	N/A	N/A	N/A	1100 °C, 6h	1 (300K) 1.8 (4.2K)	N/A	0.2 (4.2 K) 0.7 (300 K)	N/A

(a) Thickness of STO.
(b) The difference between two CNP points depending on the direction of gate voltage sweep.
(c) The gate voltage required to increase the current at CNP twice.
(d) The gate voltage for quantum Hall state corresponding to $\nu = 2$.

Table S1. Summary of comparison of the STO-graphene system between this work and literature.

REFERENCES

(1) Peres, N. M. R. *Rev. Mod. Phys.* **2010**, 82, 2673-2700.

(2) Stauber, T.; Peres, N. M. R.; Guinea, F. *Phys. Rev. B* **2007**, 76, 205423.

(3) Wehling, T. O.; Yuan, S.; Lichtenstein, A. I.; Geim, A. K.; Katsnelson, M. I. *Phys. Rev. Lett.* **2010**, 105, 056802.

(4) Ferreira, A.; Viana-Gomes, J.; Nilsson, J.; Mucciolo, E. R.; Peres, N. M. R.; Castro Neto, A. H. *Phys. Rev. B* **2011**, 83, 165402.

(5) Couto, N. J. G.; Sacepe, B.; Morpurgo, A. F. *Phys. Rev. Lett.* **2011**, 107, 225501.

(6) Saha, S.; Kahya, O.; Jaiswal, M.; Srivastava, A.; Annadi, A.; Balakrishnan, J.; Pachoud, A.; Toh, C. T.; Hong, B. H.; Ahn, J. H.; Venkatesan, T.; Ozyilmaz, B. *Sci. Rep.* **2014**, 4, 6173.

(7) Sachs, R.; Lin, Z. S.; Shi, J. *Sci. Rep.* **2014**, 4, 3657.